Measurement of ion energy distributions at the powered rf electrode in a variable magnetic field

A. D. Kuypers and H. J. Hopman
FOM Institute for Atomic and Molecular Physics, Kruislaan 407, NL-1098 SJ Amsterdam, The Netherlands

(Received 10 August 1989; accepted for publication 23 October 1989)

High-resolution energy distributions of ions, accelerated by the sheath at the powered electrode of a low-pressure 13.56-MHz gas discharge, have been measured. The observed spectra are compared to existing models. Excellent agreement between measured and calculated spectra is obtained. Detailed information on rf sheath behavior is derived from the observed energy profiles and from the measured total ion current densities towards the electrode surface. Analogous to the case of dc discharges, a decrease of sheath thickness is observed when a homogeneous variable magnetic field ($0 \leqslant B \leqslant 315$ G) is applied. However, the product of magnetic-field strength B and sheath thickness d is found to be independent of sheath voltage. This leads to the conclusion that in rf discharges, sheath contraction under influence of a magnetic field proceeds by a different mechanism than in dc discharges. It is suggested that the value of the product Bd is determined by the (virtually constant) temperature of the plasma electrons, rather than by the energy of secondary electrons that have been liberated from the electrode surface by ion bombardment. The decrease of sheath thickness d with magnetic-field strength B leads to a changing capacitive-voltage division of the applied generator voltage over the discharge. When the magnetic-field strength is sufficiently high, this may result in a sign reversal of the electrode self-bias voltage.

I. INTRODUCTION

A. Motivation of this study

The use of high-frequency discharges for surface modification of semiconductor materials is still a relatively new field. The development of micron- and submicron-scale electronic circuits, where the demand for improved pattern definition implied the need for highly anisotropic etching processes, has led to a rapid development of this technique.[1,2]

Reactive-ion etching combines the selectivity of chemical processes with the anisotropy of ion and electron bombardment of the surface. From beam experiments it is known that the energetic particles can influence gas-surface reactions in several ways. Possibilities are, for example, the creation of active surface sites by sputtering, the supply of a threshold energy for the chemical reaction, or the removal of reaction products from the surface.[3] The plasma etching process is generally a complicated (and for most cases unresolved) combination of such mechanisms. However, it is clear that energetic ion bombardment plays an important role in the etch behavior.

The energy of the ions is largely determined by the dc voltage difference between the plasma and the substrate. In the case of capacitively coupled rf discharges, negative substrate potentials of several hundreds of volts are typical.[2] These high values give rise to substantial radiation damage in the substrate surface, deteriorating electrical properties of underlying layers and contact surfaces.[4–6] Therefore it is important to have better control of the ion energies and to be able to measure them, in order to study how ion energy is related to etch rate, substrate damage, anisotropy, and selectivity.

This article describes the use of a dedicated energy analyzer at the powered rf electrode to analyze the energy distributions of ions, which have been accelerated by the sheath potential. In addition, the sheath potential can be varied by application of a homogeneous magnetic field. After an introduction, where the experimental apparatus is presented, some necessary theoretical background is given before the experimental results are shown. The theory consists of two parts. In the first part, a model is presented to calculate the energy distributions of ions after their acceleration by an rf-modulated sheath potential. In the second part, it is shown how the sheath potentials are related to the electrode voltages. Then the model is tested, and a comparison between measured and calculated spectra is made. Having established the validity of the model describing the energy spectra, this model will be used to extract detailed information about sheath potentials and ion flux from the measured data. Experimental observations of sheath behavior, both with and without application of a variable, homogeneous magnetic field, are reported and discussed.

B. rf sheath generation

When the rf power supply of a discharge is coupled to the electrodes in series with a capacitor, a large dc electrode voltage develops in addition to the applied generator voltage. This effect is referred to as self-biasing. Self-bias is caused by the difference in mobility between electrons and ions. Ions are too heavy to respond to an electric field that is oscillating at rf frequencies, while the electrons are able to follow the field fluctuations and thereby oscillate in energy. In the case considered here (generator frequency $\omega = 2\pi \times 13.56 \times 10^6$ s^{-1}), the plasma is operated in a regime where $\omega_i \leqslant \omega < \omega_e$ (with ω_i and ω_e representing the ion and electron plasma

 0021-8979/90/031229-12$03.00

frequency, respectively). Because of their higher velocity, the electrons will tend to leave the discharge much faster than the ions. This causes an excess of negative charge on the electrode surfaces, giving rise to a negative dc offset voltage. In the case of capacitively coupled discharges no net direct current can flow through the circuit, so the total electron and ion currents toward the electrode must cancel. Therefore, an equilibrium will be reached, where positive ions are almost continuously being accelerated towards the powered electrode by the negative self-bias potential. On the other hand, electrons are repelled by this potential. Only during a short fraction of an rf period will the sum of dc and rf potential be close to zero, such that electrons can reach the electrode.

When a magnetic field of a few hundred gauss is applied, parallel to the electrode surface, the mobility of the electrons in radial direction will be decreased by their Larmor precession, while the ions are virtually unaffected by the magnetic field. This means that, due to the magnetic field, current equilibrium will take place at smaller self-bias voltages.[7,8]

Therefore, variation of the strength of such a magnetic field gives control over the potential difference between plasma and electrode, which in turn determines the energy of the ions hitting the surface.

II. EXPERIMENT

A. The cylindrical magnetron reactor

The plasma chamber used in this experiment is shown schematically in Fig. 1. It consists of two coaxial aluminum cylinders, 30 cm long and of 10- and 20-cm radius, respectively. Two opposing sides of the inner cylinder are flattened so that on each surface a 3-in. wafer can be mounted vertically. The outer cylinder is grounded, the inner is capacitively coupled by a matching network to a 5-kW rf source of 13.56 MHz. Gas discharge takes place between the two cylinders. The plasma chamber is pumped to an operating pressure of typically several mTorr, while the volume inside the inner electrode is differentially pumped down to 10^{-6} Torr.

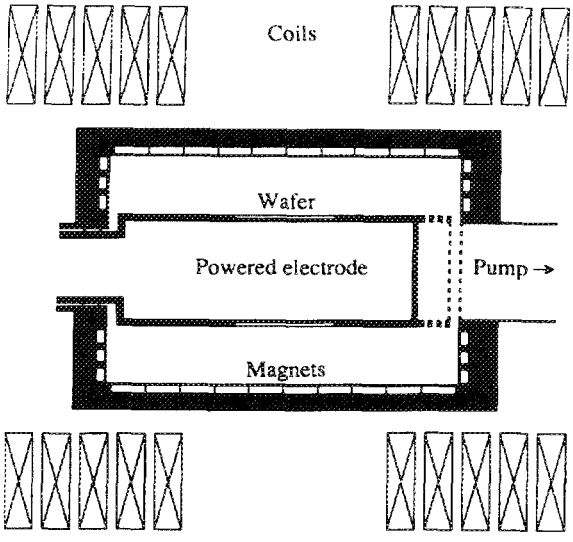

FIG. 1. Schematic cross section of cylindrical discharge geometry with magnetic fields (cylinder axes are horizontal in the figure).

A variable magnetic field is generated along the cylindrical axis by two sets of coils in a Helmholtz configuration. Field strength can be varied from 0 to 315 G.

The combination of the radial electric field E_{rf} with an axial magnetic field B causes a Larmor precession of the charged particles in the discharge. This prevents the electrons from moving directly to the electrodes, as they would when only the rf field were present. Thus, the lifetime of these electrons is enhanced considerably, along with their ability to ionize the etch gas. This effect of the magnetic field on plasma density and etch rates has been described in a previous article.[9]

In addition to this homogeneous variable magnetic field, a multipole field along the surface of the grounded electrode is generated by permanent magnets. Its construction and consequences have been described previously.[9] The point of relevance to the work discussed here is primarily that it results in a higher plasma density. In addition, it may modify the sheath properties at the grounded electrode. However, under most conditions the sheath potentials there will be low compared to those at the powered electrode.

B. The parallel-plate energy analyzer

Through a hole in the substrate surface, that is, at the powered rf electrode, incident ions are collected for direct energy analysis by an analyzer that has been mounted inside the inner cylinder.[10] Although additional information on ion mass is desirable, an electrostatic parallel-plate analyzer was chosen because of the complicating axial magnetic field. The analyzer could not be screened against this field, because the use of mu metal or compensating B fields would directly influence the orientation of the field lines in the plasma itself. This would cause unacceptable nonuniformities both in the discharge and at the substrate surface. The consequences of the magnetic field for the interpretation of the measured data are discussed below. Screening against disturbing electric fields is provided by the construction of the electrode itself: the closed inner cylinder acts as a Faraday cage, and the analyzer is at the same potential as the electrode.

In order to control the voltage applied to the plates and to measure the ion current, a connection from the powered electrode to ground had to be provided. For this purpose optical fiber coupling was chosen because it made electrical filtering against the rf and dc electrode voltages unnecessary. A more detailed description of the analyzer setup has been given elsewhere.[10]

The applied axial magnetic field strength is varied from 0 to 315 G. Combined with the fact that the voltage difference V_e between plasma and wall under normal conditions is limited to about 500 V, Larmor radii r_L of typically a meter or less are obtained in the case of singly charged Ar. Therefore, the influence of the applied magnetic field on the ion trajectories through the analyzer has to be taken into account. (The path length of the ion trajectory through the analyzer is in the order of 10 cm.) To be able to relate the field strength between the analyzer plates to the actual kinetic energy of the ions being transmitted, an analytical expres-

sion has been derived for the ion trajectory through the analyzer[11] as a function of ion mass M, magnetic field B, and electric field strength ϵ between the analyzer plates. Using this expression, the measured values of ϵ are converted to absolute ion energies by a personal computer.

III. THEORY

A. Model for the ion energy distribution

Most of the work that has been done on the analysis of ions reaching the electrode surfaces of an rf discharge has been performed at the grounded electrode. The first attempt to model the ion acceleration in an rf sheath was made in order to explain the unexpected behavior of ions extracted from a Thoneman rf ion source.[12] The energy spread of the ion beams was one or two orders higher than thermal, and mean ion energies several hundreds of volts higher than the extraction voltage were detected.[13] The higher mean energy was attributed to the large dc sheath potentials developed in rf discharges. Theoretical work by several authors[14–16] showed that in addition to the dc accelerating term, the ions are also sensitive to the rf modulation of the sheath potential. The time it takes an ion to cross the sheath is of the same order as an oscillation of the rf field. Therefore, the final energy of the ion will be determined by the phase of the field at the moment that it entered the sheath. This causes a broadening of the ion energy distribution. Assuming a sinusoidal time dependence of the sheath potential V, the total width ΔE of the energy profiles was shown[14] to be given by $\Delta E = (8e\lambda V_e/3\omega d)(2eV_e/M)^{1/2}$. Here V_e, d, M, and ω represent time-averaged sheath voltage, sheath thickness, ion mass, and the angular frequency of the rf field, respectively. (The parameter λ, describing the relative magnitude of the rf and dc components of the electric field, will be discussed below.) This theoretical result has been confirmed experimentally in rf glow discharges at the grounded electrode by other authors.[17–21] However, the assumptions underlying these models were not self-consistent.[22] Recently, the model has been improved by Vallinga and Meijer.[22,23] It will be used here to interpret the measurements.

The following assumptions are made in this model:

(1) The ion acceleration is predominantly determined by the time-averaged sheath potential, and the rf contribution can be considered as a perturbation.

(2) The ion sheath thickness is constant in time.

(3) Free fall of ions through the sheath, i.e., the ion mean free path $l > d$.

(4) Contribution of electrons to the total space charge in the sheath can be neglected.

(5) The number of ions entering the sheath is constant in time.

(6) The initial velocity of ions entering the sheath can be neglected.

(7) The ion transit time τ across the sheath is approximately constant, i.e., independent of the phase of the electric field upon entering the sheath.

(8) The sheath potential can be approximated by

$$V(x,t) = V_e[1 + \lambda \sin(\omega t)][(x/d)^n - 1], \qquad (1)$$

where x denotes the distance perpendicular to the electrode surface, and λ and n represent parameters that will be discussed below. Under these assumptions, the equation of ion motion was solved analytically, and the following relation for the ion energy at the electrode was obtained:

$$E \approx eV_e\left(1 - \frac{\lambda n}{\omega d}\sqrt{\frac{2eV_e}{M}}(\sin \omega t_1 - \sin \omega t_0)\right), \qquad (2)$$

where t_0 and t_1 are the moments of entering the sheath and reaching the electrode surface, respectively. Thus the theoretical broadening of the energy distribution is given by

$$\Delta E = E_{\max} - E_{\min} = 4a\left[\lambda n (eV_e)^{3/2}/\omega d\sqrt{2M}\right], \qquad (3)$$

where $a = \max|\sin\omega t_1 - \sin\omega t_0|$. Under assumption 7, given above, the ion transit time $\tau = t_1 - t_0$ is constant. Then, $a \leqslant 2|\sin(\omega\tau/2)|$. When it takes an ion several rf field oscillations to cross the sheath ($\tau > 2\pi/\omega$), it will be assumed [23] that, on the average, $a = 1$.

As a final result, the ion energy distribution is given by[14]

$$F_i(E) = \frac{4N_0}{\omega\Delta E}\left[1 - \left(\frac{2(E - eV_e)}{\Delta E}\right)^2\right]^{-1/2}, \qquad (4)$$

for $(eV_e - \Delta E/2) \leqslant E \leqslant (eV_e + \Delta E/2)$ and $F_i(E) = 0$ elsewhere. Here N_0 represents the number of ions entering the sheath per unit time. The profiles described by Eq. (4) are symmetric around the mean energy value $E = eV_e$. An example of a profile as described by Eq. (4) is given in Fig. 2 for a typical choice of parameters. The applicability of the assumptions 1 to 8, given above, to the discharge under consideration will be discussed below. However, further assumptions have to be made about the constants λ and n in Eqs. (1)–(3).

B. Model for parameter λ

The constant λ determines the relative magnitude of the dc and the rf component of the sheath voltage. The sheath potential V_e can be measured directly, but λ has to be esti-

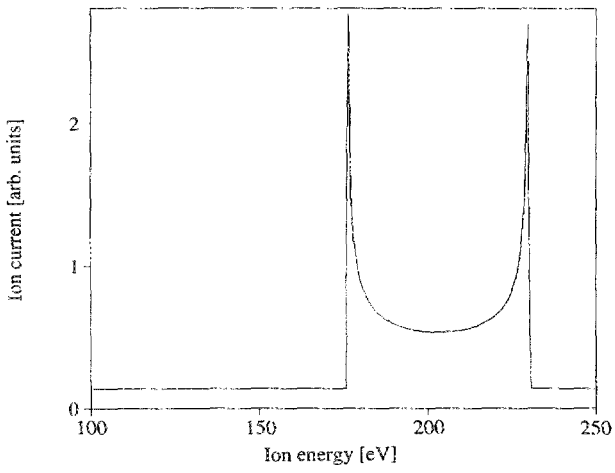

FIG. 2. Energy profile, calculated from Eq. (6) for a typical choice of parameters (compare with measured spectrum in Fig. 5).

mated. To do this, a model will be used here, as presented by Keller and Pennebaker.[24] Assume that the sheath potential is given by $V = V_e + \lambda V_e \sin(\omega t)$ [Eq. (1)]. Then, if the electrons have a Maxwell–Boltzmann energy distribution of temperature T_e, the time-averaged electron current density $\langle J_e \rangle_t$ through the sheath is given by[25]

$$\langle J_e \rangle_t = J_{e0} I_0(e\lambda V_e / kT_e), \tag{5}$$

where J_{e0} is the current density which would be drawn if $\lambda = 0$,

$$J_{e0} = J_{esat} \exp(eV_e / kT_e), \tag{6}$$

and I_0 is the zeroth-order modified Bessel function of the first kind. In the steady-state situation, the time-averaged ion and electron currents across the sheath must cancel. Thus, the average electron current density must be equal to the ion current density J_i. Together with Eqs. (5) and (6), this gives

$$\exp(-eV_e/kT_e) = J_{esat} I_0(e\lambda V_e/kT_e)/J_i. \tag{7}$$

When $\lambda = 0$, this equation reduces to the equation for the floating potential V_f, as will be discussed below. Defining

$$V_e = \Delta V_e + V_f, \tag{8}$$

the change in dc potential due to the presence of the rf voltage, ΔV_e, is given by[24]

$$\exp(e\Delta V_e/kT_e) = I_0(e\lambda V_e/kT_e), \tag{9}$$

which for $e\lambda V_e/kT_e \gg 1$ reduces to[24]

$$\Delta V_e/\lambda V_e = -1 + (kT_e/2e\lambda V_e)\ln(2\pi e\lambda V_e/kT_e). \tag{10}$$

For a typical electron temperature $T_e \approx 3$ eV and ion temperature $T_i \approx 0.04$ eV (room temperature), the floating potential[26] V_f is in the order of 10 to 20 V. On the other hand, the observed sheath potentials V_e at the powered electrode are typically in the order of a few hundred volts. Thus, $V_f \ll V_e$, and it follows from Eq. (8) that $V_e \approx \Delta V_e$. Physically speaking, it means that the dc component of the sheath potential is determined primarily by the rf-induced term. Further, for this kind of large value for V_e, it follows from Eq. (10) that $\Delta V_e \approx -\lambda V_e$. It is concluded that, as long as $V_e \gg V_f$, $\lambda \approx -1$. However, in the case of small sheath voltages, combination of Eqs. (8) and (10) shows that λ is given by

$$\lambda = (-V_e + V_f)/V_e. \tag{11}$$

To interpret the measurements, this model has to be extended with a relation between the sheath potential V and the applied generator voltage V_a at the powered electrode. For this purpose, a sheath model developed by Kohler[27] will be used here. Assume that the electron current in the sheath can be divided into a dc and an rf term:

$$J_e(t) = \langle J_e \rangle_t + J_d(\omega t) = J_i + J_d \sin(\omega t). \tag{12}$$

(As above, the fact that the average electron current density $\langle J_e \rangle_t$ is equal to the ion current density J_i has been used here). J_d stands for the displacement current density, associated with the oscillatory electron movement in the rf field. When $J_i \ll J_d$, the sheath essentially acts as a capacitor. In that case, the discharge can be modeled by an equivalent electrical circuit, where the electrode sheaths are represented by capacitors (Fig. 3).

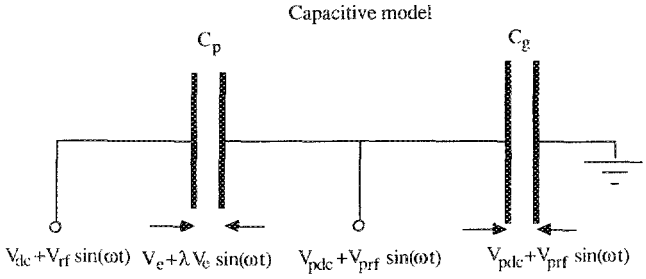

FIG. 3. Equivalent electrical circuit for the discharge, where the sheaths are assumed to be purely capacitive, and the plasma bulk is assumed to be perfectly conducting. As a result, the potential of the plasma is equal to the potential drop across C_g.

C. Capacitive sheath approximation

Let C_p and C_g be the capacitances of the sheaths at the powered and the grounded electrode, respectively (Fig. 3). The plasma bulk is considered to be a perfect conductor with zero resistance. The potential difference between the powered and the grounded electrode is capacitively divided over both sheaths. Consequently, when the applied generator voltage is given by

$$V_a(t) = V_{dc} + V_{rf} \sin(\omega t), \tag{13}$$

the plasma potential $V_p(t)$ will also show a purely sinusoidal behavior:

$$V_p(t) = V_{pdc} + V_{prf} \sin(\omega t). \tag{14}$$

(See Fig. 4.) The sheath potential at the grounded electrode is then given by the voltage drop over C_g, which is just $V_p(t)$.

One implication of Eq. (11) is that the plasma always exceeds the electrode potentials by at least an amount V_f.

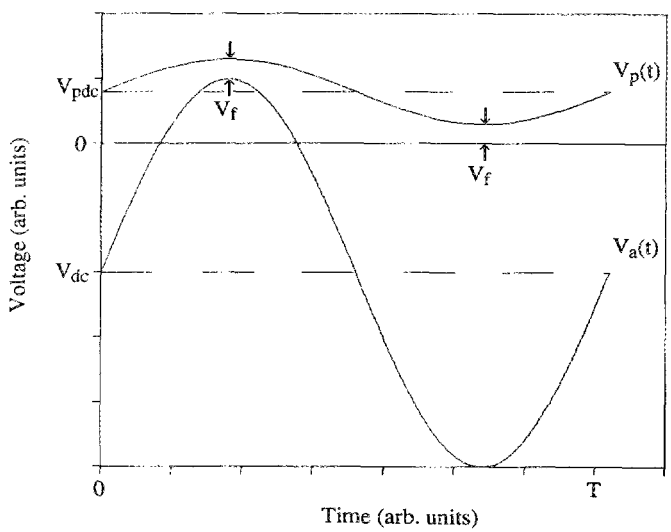

FIG. 4. Applied electrode potential $V_a(t)$ and plasma potential $V_p(t)$ relative to ground, according to the capacitive sheath model. $V_a = V_{dc} + V_{rf}\sin(\omega t)$, and $V_p(t) = V_{pdc} + V_{prf}\sin(\omega t)$. The potential drop across the sheath is just $V_p(t) - V_a(t) = V(t) = V_e + \lambda V_e \sin(\omega t)$.

(Because V_f is defined as being positive, it means that the plasma is always more positive than any surface in contact with it. This is a direct consequence of the fact that the drift velocity of electrons is much higher than that of ions.) Using this implication, it follows from Eqs. (13) and (14) that[27]

$$V_p(t) = V_f + \tfrac{1}{2}(V_{dc} + V_{rf})[1 + \sin(\omega t)]. \quad (15)$$

(See also Fig. 4.) The sheath potential at the powered electrode is equal to the potential drop over C_p (Figs. 3 and 4):

$$V(t) = V_e[1 + \lambda \sin(\omega t)] = V_p(t) - V_a(t).$$

This leads to the following results:

$$V_e = \tfrac{1}{2}(V_{rf} - V_{dc}) + V_f \quad (16)$$

and

$$\lambda = -\frac{\frac{1}{2}(V_{rf} - V_{dc})}{\frac{1}{2}(V_{rf} - V_{dc}) - V_f}. \quad (17)$$

Note that, generally, V_{dc} is negative. Now that both sheath potentials $V(t)$ and $V_p(t)$ can be directly related to the generator voltage V_{rf} and the electrode offset V_{dc}, it is useful to have a relation connecting the two last mentioned. It follows directly from the capacitive voltage division of the applied-rf amplitude V_{rf} that the rf component of the plasma potential is given by[27] $V_{prf} = V_{rf}[C_p/(C_p + C_g)]$. Combining this with Eq. (15) then gives

$$V_{dc} = V_{rf}[(C_p - C_g)/(C_p + C_g)]. \quad (18)$$

A larger electrode area results in a higher electrode sheath capacitance.[28] Thus, in the reactor considered here, the sheath at the grounded electrode has the largest capacitance: $C_g \gg C_p$. It follows from Eq. (18) that $V_{dc} \approx -V_{rf}$. Neglecting V_f in cases that $V_{rf} \approx |V_{dc}| \gg |V_f|$, it then follows from Eq. (17) that again $\lambda \approx -1$, as was obtained earlier above.

D. Value of parameter n

The constant n [in Eqs. (3)–(5)] determines the dependence of the sheath potential on the distance x to the electrode surface. When the gas pressure is so low that the ion mean free path is larger than the sheath thickness ($l > d$, assumption 4), a free-fall model can be used. In this case,[26] $n = \frac{4}{3}$. When in addition $\lambda = -1$ and $a = 1$, Eq. (5) reduces to

$$\Delta E = \frac{8}{3\omega d}[(eV_e)^{3/2}/\sqrt{2M}]. \quad (19)$$

In the following, this formula will be used as a first attempt to interpret the measured energy profiles, and all other regimes and choices of constants will be considered as deviations from this ideal case. In this regime ($n = \frac{4}{3}$) the Langmuir–Child space-charge-limited current equation for the total ion flux towards the electrode is also valid[26]:

$$J_i = \frac{4\epsilon_0}{9}\sqrt{\frac{2e}{M}}\frac{V_e^{3/2}}{d^2}. \quad (20)$$

When both $E(= eV_e)$ and J_i are measured, this can be used to check the validity of Eq. (19) because both equations have to be consistent: the value of the time-averaged sheath thickness d, which can be obtained from Eq. (16), has to give the right value for J_i when inserted into Eq. (20).

IV. MEASUREMENT OF ENERGY DISTRIBUTIONS FOR $B = 0$

A. Shape of the ion energy distribution

In the following experiments, a 0.5-mm-thick aluminum dummy wafer with a 200 μm hole with knife edges was used to extract the substrate bombarding ions for energy analysis. Instead of operating as an energy analyzer, the complete analyzer can also be used as one big Faraday cup. The total ion current collected by the diaphragm can then be measured. From this, the ion flux J_i towards the surface of the powered electrode can be derived.

Parallel to these measurements, the dc offset of the powered electrode has been recorded using an oscilloscope. A probe with an attenuation factor of 1000 was connected to the electrode, and the signal was measured relative to ground potential. From the dc shift of the sinusoidal oscilloscope trace the value of V_{dc} was obtained.

A typical result of an energy spectrum, obtained from a discharge at 2.4-mTorr argon gas pressure, is shown in Fig. 5. The shape of the measured profile resembles the calculated distribution given in Fig. 2. However, two differences between both figures are obvious. First, the measured profile is slightly asymmetric, and second, the slope of the edges is not infinite. These observations can be accounted for by the limited energy resolution of the analyzer. The measured profile is a convolution of the calculated profile and the response characteristics of the analyzer. When the analyzer is scanned to measure the ion distribution, not only ions with energy E will be collected, but also particles of slightly different energy. This explains the finite slope at the edges of the profile. In addition, it is assumed that the energy analyzer has a Gaussian energy window of full-width-half-maximum ΔW. It is known[29] that $\Delta W/E$ is constant for a given analyzer geometry. This means that the sensitivity of the apparatus increases with E, because ions from a larger energy window are col-

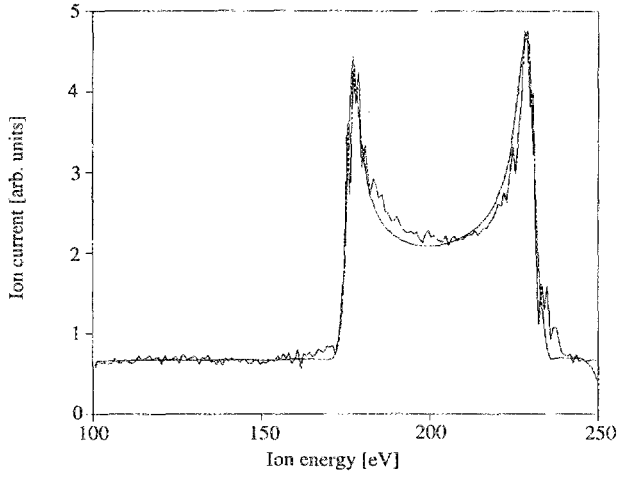

FIG. 5. Measured ion energy distribution in 2.4-mTorr argon ($B = 0$, rf power 1 kW). Mean ion energy $E = 203$ eV, energy width $\Delta E = 54$ eV. The smooth line has been obtained by convoluting the calculated profile in Fig. 2 with a Gaussian energy window of FWHM $\Delta W(E)$, to account for the energy dependence of the analyzer detection efficiency. Plotted line corresponds to best fit, obtained for $\Delta W(E) = 0.016E$.

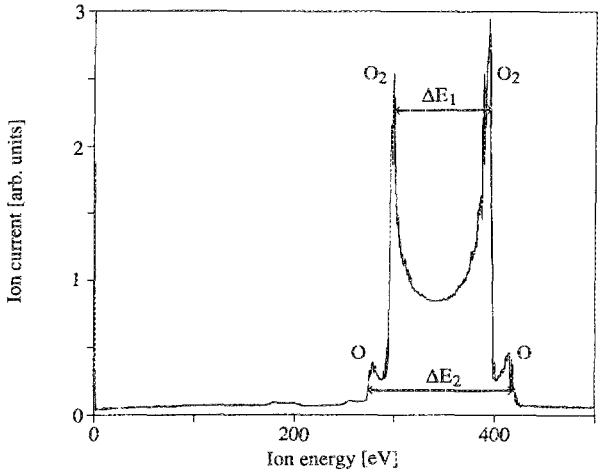

FIG. 6. Measured ion energy distribution in 3-mTorr oxygen ($B = 0$, rf power 1 kW). $(\Delta E_2/\Delta E_1)^2 \approx 2$.

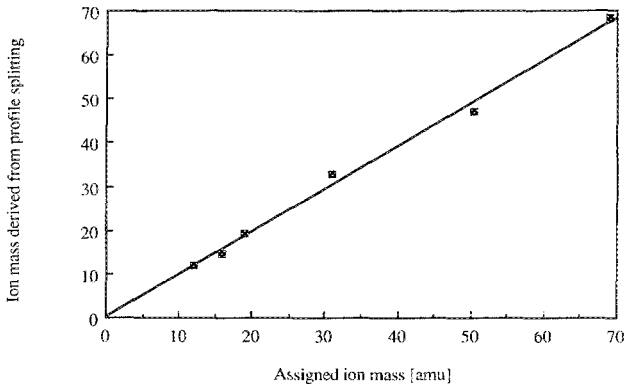

FIG. 8. Ion mass as obtained from the observed energy splittings in Fig. 7, plotted as a function of assigned ion mass.

lected. Therefore, a symmetric ion energy distribution will result in a measured spectrum with higher intensity at the high-energy side. This explains the observed asymmetry. (When the curve, given in Fig. 2, is convoluted by a Gaussian energy window with a fitted FWHM of $\Delta W(E) = 0.016E$, the calculated line in Fig. 8 is obtained.) Residual differences may be attributed to small deviations from sinusoidal time dependence of the sheath potential.

B. Mass effect

From Eq. (19) it is expected that the width ΔE of the energy profile scales with $M^{-1/2}$. To check this, profiles have been measured in different molecular gases. A typical result obtained in an oxygen discharge is shown in Fig. 6. Two profiles of widths ΔE_1 and ΔE_2 are superimposed. Their relative magnitude is given by $(\Delta E_2/\Delta E_1)^2 \approx 2$, so $M_1 \approx 2M_2$. It is concluded that the inner peak represents O_2^+ molecules, and the outer peak O^+ atoms, produced by dissociation in the discharge. This leads to the remarkable result that, although the analyzer only measures energy, also mass selection is obtained, because of the different response to the rf component of the sheath potential with ion mass.

A similar effect is observed in a CF_4 discharge. Figure 7 shows a spectrum measured at a relatively high rf power of 3 kW. Because the value of d in Eq. (19) is not known, absolute values for the different ion masses can only be obtained by tentatively attributing one peak to a certain mass, and then verifying whether the other peaks correspond to masses that are to be expected from a CF_4 discharge. The assignment of the peaks in Fig. 7 was obtained by attributing the largest splitting to C^+ ions. (The second C^+ peak is missing in the observed spectrum in Fig. 7, because of the limited scan range. The distance of the first C^+ peak to the middle of the profile was used to find ΔE_{C^+}.) The mass thus calculated from the measured splittings has been plotted as a function of assigned ion mass in Fig. 8. It is concluded that the corre-

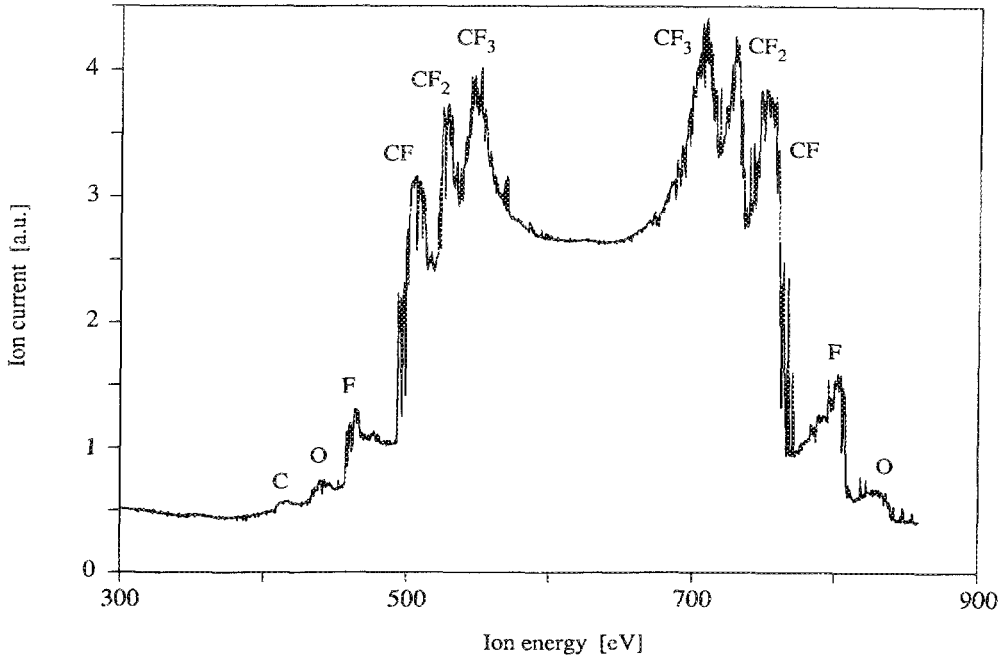

FIG. 7. Measured ion energy distribution in 3-mTorr CF_4 ($B = 0$, rf power 3 kW).

lation is very good, in contrast to observations by other authors.[18,30]

The spectra in Figs. 5, 6, and 7 are all symmetric around a mean energy value E. This confirms the assumption that acceleration by the rf component of the sheath potential can be treated as a second-order effect, in addition to the acceleration by the dc potential. However, ions collected from a discharge in a mixture of argon and hydrogen show an energy distribution as given by Fig. 9. Peak assignment was performed as above. The middle of the Ar profile is taken as the mean energy E. Then for all three hydrogen profiles, it is observed that the high-energy peaks are located further away from E than the corresponding low-energy peaks. This is explained by the low mass of the H atoms and molecules. From the Ar profile, a sheath thickness $d = 3.9$ mm is obtained, using Eq. (19). When the traversion time τ for an Ar atom of energy $E(= 334$ eV) is calculated by a computer-trajectory calculation, it appears that it takes more than four rf oscillations to cross the sheath. The same calculation for an H atom gives values from 0.3 up to about 0.7 oscillations. This means that the Ar atom predominantly experiences a time-averaged sheath potential, while the H atom responds to an almost instantaneous potential. Clearly, assumptions 1 and 7 in the analytical treatment above break down for the case of hydrogen. When the H atom enters the sheath at a moment that the sheath potential becomes high, it crosses the sheath very fast. In principle, it can be accelerated to an energy $E \leqslant 2E$. Note that in Fig. 9 the H^+ energy distribution extends almost exactly to this ultimate value. However, when the H atom enters the sheath when the potential becomes low, it will take a considerable part of an rf oscillation to cross the sheath. Therefore, its final energy will be closer to the time-averaged value E.

V. ION ENERGY MEASUREMENTS AT CONSTANT POWER FOR $B > 0$

At a constant absorbed power of 500 W, the influence of the variable axial magnetic field on electrical discharge characteristics has been studied. Field strength was varied from 0 to 315 G. Measured values of V_{dc}, V_{rf}, and $V_e (= E/e)$ have been plotted as a function of B in Fig. 10.

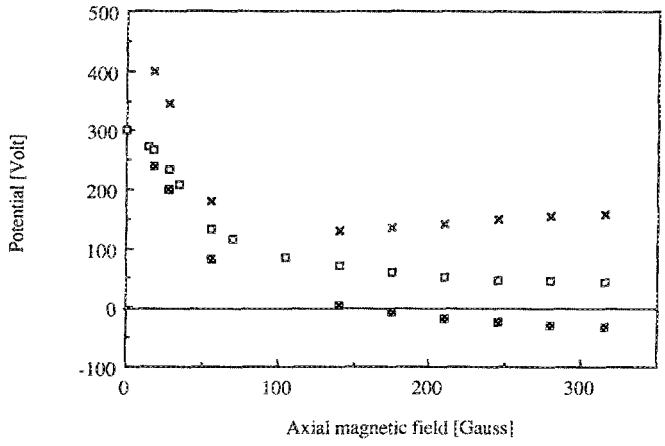

FIG. 10. dc (black squares) and rf (crosses) components of applied electrode voltage, together with time-averaged sheath voltage V_e (open squares), measured in 2.4-mTorr argon (constant rf power 500 W).

The physical meaning of Fig. 10 is clear: the electron diffusion in the direction of the electric field decreases with increasing magnetic-field strength. Therefore, equilibrium between the time-averaged ion and electron currents towards the electrode will be reached at a lower sheath potential. This will be discussed in more detail below, together with the measurements performed at constant amplitude V_{rf}.

The total ion current density, both as measured and as calculated from the ion-energy profiles [using Eqs. (19) and (20)], is given in Fig. 11. It should be noted that the measured current densities at magnetic-field strengths above 100 G, are higher than reported in a previous publication.[31] In the case of a 200-μm diaphragm in front of the energy analyzer it was observed that, under certain conditions, not only ions, but also electrons, were able to enter the detection volume. Therefore, the measurements of ion current density

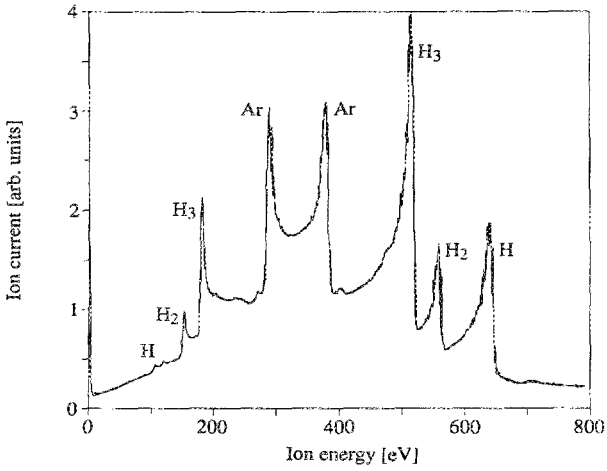

FIG. 9. Measured ion energy distribution in a 3-mTorr mixture of argon and hydrogen (5 sccm H_2 + 2 sccm Ar, $B = 0$, rf power 2 kW).

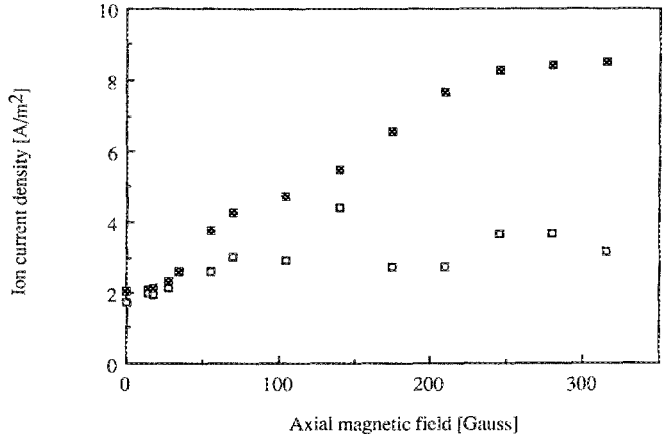

FIG. 11. Filled squares: measured ion flux to the powered electrode surface. Open squares: flux as calculated from observed energy splittings, assuming $\lambda = 1$ (discharge conditions as in Fig. 10).

have been repeated with a smaller (50-μm-diam) diaphragm. After this modification, the measured ion current densities for $B < 100$ G were unaltered. However, for $B > 100$ G, now a continued increase of J is observed with B (instead of the saturation mistakenly reported earlier).[31]

This observed increase of J with magnetic field strength is obviously related to a similar increase of the ion density in the plasma bulk, which has been measured with a Langmuir probe.

Although the calculated current density gives good agreement with experimental values at low-magnetic-field strengths, above 100 G the calculated values are clearly much too low. This apparent discrepancy can be explained as follows. First, it should be noted that there is no reason to assume that the equation for space-charge-limited current [Eq. (20)] does not hold anymore. At higher B values, ion movement is still collisionless and also, the Lorentz force acting on the ions is much smaller than the Coulomb force due to the sheath electric field. Therefore, Eq. (20) remains valid. To calculate J_i from Eq. (20), values for V_e and d are substituted. The sheath potential V_e is well known, because it is directly obtained from the energy profiles. Therefore, the observed discrepancy must be due to an error in the determination of the sheath thickness d. So far, all values for d have been derived from the observed energy splittings ΔE, using Eq. (19). However, in this equation it is assumed that $\lambda = 1$, and this is only justified when $V_e \gg V_f$ [Eq. (8)]. Apparently, this condition is violated as V_e decreases with B (Fig. 10).

For $0 \leqslant B < 50$ G, good quantitative agreement is obtained between the measured ion flux and the fluxes which are calculated with Eqs. (19) and (20) [see Figs. 11 and 15(a), and also a previous publication[10] which deals exclusively with the case $B = 0$]. Thus, it has been established that the parameter d is indeed the same in both equations. Therefore, it is now allowed to reverse the procedure: Instead of calculating d from Eq. (19) in order to obtain J_i, the measured values of J_i and V_e can be used to find d [Eq. (20)]. To calculate λ from d, Eq. (3) should be used instead of Eq. (19). The parameters n and a, appearing in Eq. (3), are not influenced by the magnetic field, because the free-fall approximation remains valid ($n = \frac{4}{3}$) and it takes an argon ion several rf oscillations to cross the sheath ($a = 1$). Following this procedure, substitution of the data presented in Figs. 10 and 11 leads to the conclusion that λ is somewhat smaller than 1, which implies that the rf component λV_e of the sheath potential is smaller than the dc component V_e. This was predicted by Eq. (8), where it has been shown that the difference between the dc and the rf component is approximately equal to the floating potential V_f.

The values of V_f, thus calculated from the experimental data, are plotted in Fig. 12. The substantial scattering in these data is due to the fact that they are obtained by subtracting two relatively large numbers. However, fitting a straight line to these data points, it is concluded that the floating potential has a value somewhere between 13 and 17 V. These are realistic values for a discharge with an electron temperature of a few eV (see Sec. III B), and thus support the statement that λ can be obtained as given above.

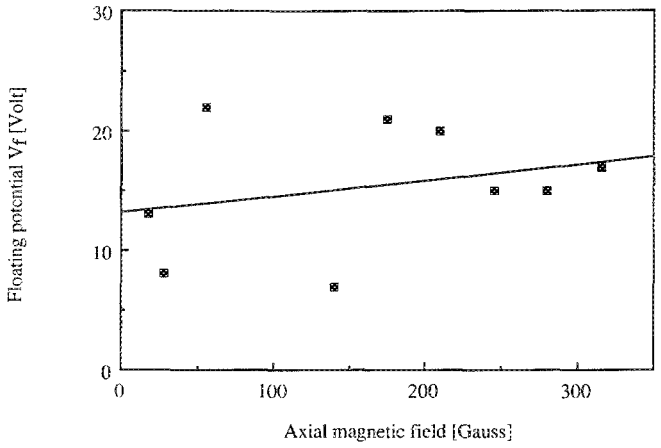

FIG. 12. Floating potential V_f, as calculated from measured ion flux and ion energy distributions (discharge conditions as in Fig. 10).

VI. MEASUREMENTS AT CONSTANT GENERATOR VOLTAGE

In the experiments presented in Sec. V, the rf power absorbed by the discharge was kept constant in order to study the response of the system to the applied axial magnetic field. However, when a detailed study is made of the effect of this magnetic field on the potentials and offset voltages, it is more convenient to keep the applied generator voltage constant. The following results have all been obtained by keeping the rf amplitude V_{rf} (as observed on the oscilloscope connected to the powered electrode) at a constant value of 232 V. This, of course, has the consequence that now the total input power is varying with B.

For a discharge in 2.4-mTorr argon, the mean energy of ions arriving at the surface of the powered electrode is given in Fig. 13. Instead of the monotonic decrease in energy, observed in the case of constant power, an initial increase as a function of magnetic-field strength is seen here. Above 100 G the ion energy becomes lower.

Also the measured dc offset voltage on the powered electrode shows a different dependence on magnetic field now

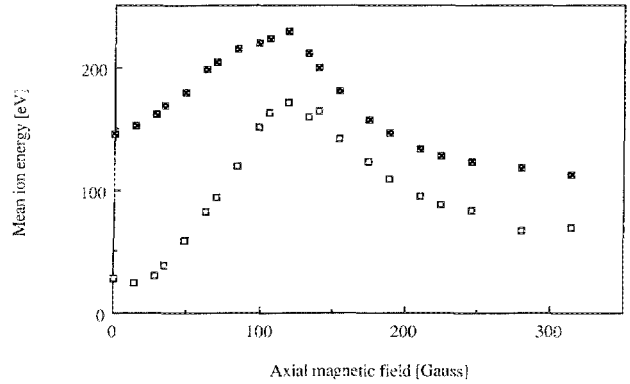

FIG. 13. Measured mean ion energy E (filled squares) and energy splittings ΔE (open squares) in 2.4-mTorr argon, at a constant electrode voltage $V_{rf} = 232$ V. (rf power between 180 and 3100 W).

that the generator voltage is kept constant. From Fig. 14 it is seen that up to 100 G, the dc offset remains remarkably constant. Only at higher field strengths again a monotonic decrease is observed, down to 0 V, and even changing sign.

As shown above, the time-averaged plasma potential $V_p = V_e + V_{dc}$. The result is also plotted in Fig. 14. It appears that above 100 G, V_{dc} and $V_e = E/e$ (Fig. 13) decrease at about the same rate, resulting in an almost constant plasma potential.

In addition, the total ion flux has been measured under the same conditions [Fig. 15(a)]. From the measured energy distributions, the splittings ΔE have been determined (Fig. 13). Substituting these values into Eq. (19) it is found that the sheath thickness shows a monotonic decrease from 5 to 1 mm. Substituting d Eq. (20) again, the ion flux can be calculated. The values thus obtained are also plotted in Fig. 15(a) for comparison. Just as in the measurements at constant power (Fig. 11) a large difference between measured and calculated flux is observed for higher magnetic-field strengths. Note that here the deviation starts at a higher magnetic-field strength ($\approx$100 G) than in the constant-power case ($\approx$40 G). This supports the conclusion that the deviation is due to a breakdown of the condition $V_e \gg V_f$, because in the former situation the sheath potentials only start decreasing near 100 G, whereas in the latter V_e decreases monotonically for $B > 0$. Following the same procedure as in Sec. V, λ and V_f can be derived from the measurements in Figs. 13 and 14. Values for V_f, scattering around 20 V ($\pm$ 15 V), are obtained.

Langmuir-probe measurements have been performed under the same discharge conditions.[11] The ion density as a function of magnetic-field strength is given in Fig. 15(b). It is observed that both the ion density n_i and the ion current density J_i show qualitatively the same behavior. At zero magnetic-field strength, an rf amplitude of 232 V is obtained at 180 W input power. Going from 0 to 130 G, the absorbed rf power has to be increased up to 3.1 kW to maintain the same rf voltage on the powered electrode. In this domain, both the ion current density towards the electrode surface and the ion density in the bulk of the plasma show a linear

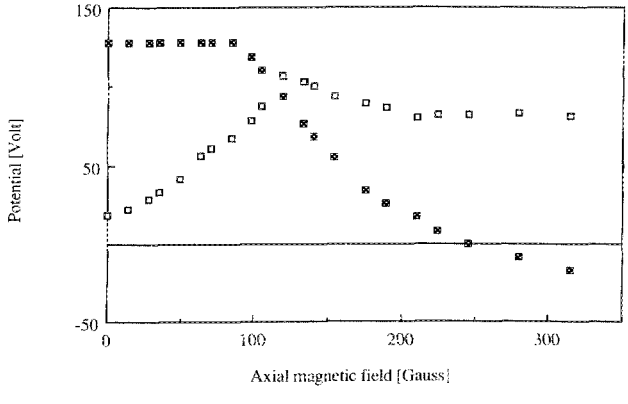

FIG. 14. Measured dc offset of the powered electrode (filled squares), together with dc component of the plasma potential (open squares), as obtained from measured V_{dc} and E by $V_{pdc} = E + V_{dc}$. Discharge conditions as in Fig. 13.

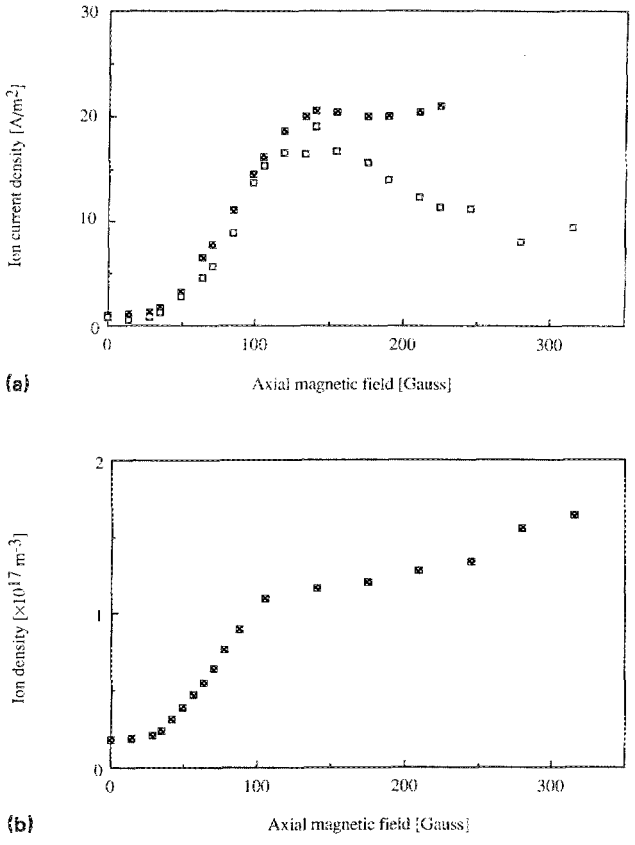

FIG. 15. (a) Measured ion flux to the powered electrode surface (filled squares), and flux as calculated from observed energy splittings, assuming $\lambda = 1$ (open squares). Discharge conditions as in Fig. 13. (b) Ion density at a distance of 4.5 cm from the surface of the powered electrode, measured by Langmuir probe. Discharge conditions as in Fig. 13.

increase with power. A further increase of the magnetic-field strength allows the supply of power to be lowered again, down to a value of 1.9 kW at 315 G. However, ion current and ion density show a further increase with B, despite the lower power levels. Thus, the knee in Figs. 15(a) and 15(b) can be explained: Below 100 G there is a combined increase of power input and electron confinement. Above this value, the effect of a further improvement of confinement is almost compensated for by a decreasing power input.

VII. DISCUSSION

A. Validity of the assumption of a capacitive sheath

First, it will be shown here that the capacitive sheath model is indeed valid under the current experimental conditions. To prove this, it has to be shown that the displacement current $J_d = A_p\, dQ/dt$ is larger than the condition current J_i.

The capacitance C of two surfaces of equal area A at a mutual distance d is given by

$$C = \epsilon_0 (A/d). \tag{21}$$

For the sheath at the powered electrode, $A = A_p$, while d is given by space-charge-limited current equation (20). Substitution into Eq. (21) gives

$$C_p = \tfrac{1}{2}(M\epsilon_0{}^2/2e)^{1/4} A_p J_i^{1/2} V_e^{-3/4}. \tag{22}$$

This relation is also given by Keller and Pennebaker.[24] Because d was shown to be independent of power ($B = 0$ and constant pressure), it follows from Eq. (21) that C_p is also power independent. Substitution of the values measured at $P = 500$ W ($V_e = 280$ V, $J_i = 1.6$ A/m^2, $A_p = 0.163$ m^2) gives $C_p = 0.3$ nF. Assuming C_p to be time independent, J_d can now be estimated:

$$J_d = C_p \frac{dV}{dt} = C_p \omega V_e \cos(\omega t). \tag{23}$$

Taking the time average, it follows that $dQ/dt = 2C_p \omega V_e/(\pi A)$. For $P = 500$ W, this gives a displacement current of 88 A/m^2. Thus it has been shown that indeed $J_i \ll J_d$, and the capacitive approximation is justified.

B. Influence of magnetic field on sheath thickness

For the nonmagnetized case, it has been shown that the sheath thickness d, derived from the observed ion energy splittings, is the same as the value determining the space-charge-limited current. In addition it has been shown that for $B > 0$, the values of d, calculated from the measured ion current densities J_i, lead to consistent results if deviations of λ from unity are taken into account. It is concluded that at the low pressures considered here, the value of d thus obtained gives a reliable absolute measure of the sheath thickness. This will be used in the following to study rf sheath behavior in a magnetic field.

For both experiments in argon, at constant power (500 W) and constant generator voltage ($V_{rf} = 232$ V), the reciprocal value of d (obtained from the measured J_i) is plotted as a function of B in Fig. 16. A striking coincidence of the results of the two experiments is observed. This is remarkable, because the sheath potentials and ion fluxes involved are entirely different for the two cases. For $B > 30$ G, a constant value of the product Bd ($= 0.134$ G m) is obtained.

A similar decrease of sheath thickness has been observed in magnetized dc discharges. At gas pressures between 0.3 and 20 Torr, the cathode dark-space thickness was measured visually in different gases by Güntherschulze[32]. He observed a gradual decrease of sheath thickness as a function of B, from 1–2 cm down to a minimum value $d = 0.7$ mm. In addition, the current density appeared to be given by $J_i = \text{const}/d^2$. No change in sheath potential was observed here. However, earlier work by Willows[33] at lower gas pressures had shown a decreasing cathode fall potential, indicating a pressure dependence. A theoretical explanation for the shrinking of the dark space was given by Thomson and Thomson.[34] It is based on the fact that the dc discharge is sustained by secondary electrons, liberated from the cathode surface by charged-particle bombardment. This theory has been adopted by many workers in the field of dc magnetrons.[35–37] Here Thomsons' results are given as reproduced by Francis.[38] The equations of motion for an electron in crossed electric and magnetic fields are given by

$$m\frac{d^2x}{dt^2} = e\epsilon - eB\frac{dy}{dt} \tag{24}$$

and

$$m\frac{d^2y}{dt^2} = eB\frac{dx}{dt}. \tag{25}$$

A linear decreasing electric field is assumed across the sheath (case $n = 2$ above), giving

$$\epsilon = (2V_e/d)[1 - (x/d)]. \tag{26}$$

With the boundary condition that for $x = 0$, $dx/dt = dy/dt = 0$, the solution of Eqs. (25) and (26) is given by

$$x = \frac{2V_e/d}{2V_e/d^2 + eB^2/m}[1 - \cos(\gamma t)] \tag{27}$$

with

$$\gamma^2 = \frac{2eV_e/d^2 + e^2B^2/m}{m}. \tag{28}$$

Under the assumption of collisionless movement, the maximum distance x_{max} the electron can reach, relative to the electrode surface, is then given by Eq. (27) with $\cos(\gamma t) = 0$. As long as $x_{max} > d$, the path length the electron travels through the sheath will only be slightly affected by B. However, when $x_{max} < d$, the electron will be bent back towards the surface, and the path length increases drastically. This causes an increasing excitation and ionization in the sheath region, reducing the observed sheath thickness. Thus a critical value B_c can be defined, above which the magnetic field will modify the sheath. It is given by the condition $x_{max} = d$. From Eqs. (27) and (28) it then follows that

$$B_c = (1/d)\sqrt{2V_e m/e}. \tag{29}$$

Recent calculations by Maniv[39] lead to a comparable result. Physically, Eq. (29) means that the Larmor radius of the electron, corrected for the accelerating field $\epsilon(x)$, is equal to d.

It is tempting to apply the same reasoning to the rf case. Substitution of relevant numbers shows that the observed rf discharge behavior might also be due to secondary electrons.[31] However, there is growing evidence that secondary electrons only play an additional role in sustaining 13.56-MHz plasmas.[11,24,40] The experimental evidence for fast electrons, originating from the sheath regions, can also be

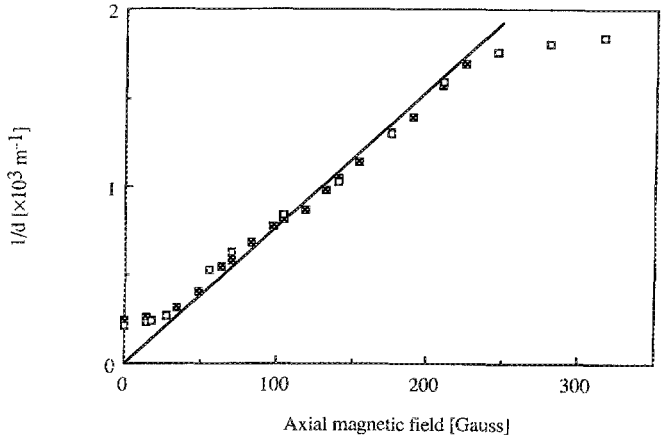

FIG. 16. Reciprocal sheath thickness, as calculated from measured ion flux, for the cases of constant power (500 W, filled squares) and constant rf voltage (232 V, open squares), respectively.

accounted for by acceleration at the oscillating plasma-sheath boundary.[41–43]

From Fig. 16 a value $Bd = 0.134$ G m is obtained. Substituting in Eq. (26), this gives a potential $V = 8$ V. It should be noted that a constant value is found, although the sheath potential V_c depends on B. This suggests that d is not determined by the ability of secondary electrons to reach the plasma, but by the condition that electrons from the plasma must be able to reach the electrode, in order to satisfy the condition $J_i + \langle J_e \rangle_t = 0$. As stated above, T_e is a few eV, and will be fairly constant under the given conditions. Most of the electron current towards the electron surface flows when $V(x,t)$ is closest to zero. Then, electrons from the tail of the Maxwell–Boltzmann distribution have to cross the sheath against the remaining negative sheath potential (which is in the order of V_f). Only when d scales with B as given in Eq. (29), will it be possible to maintain zero net current.

The ion current density J_i is determined by the ion drift towards the plasma-sheath boundary, as argued above. From Figs. 15(a) and 15(b), it follows that $J_i \propto n_i$. Therefore, J_i depends on B via the growing plasma density, which in turn is a consequence of improved charged-particle confinement. Then the space-charge-limited current Eq. (20) explains the behavior of V_c, and thus E, with B.

C. Capacitive-voltage division and sign reversal of dc offset on powered electrode

The development of the dc component of the plasma potential, V_{pdc}, is determined by the sheath behavior at the grounded electrode. In order to say something quantitative about this, two assumptions have to be made. First, it is assumed that the ion drift towards both electrodes is equal. This assumption is supported by the knowledge that J_i is not depending on the sheath potential. Second, it is assumed that there is no dc potential drop across the plasma volume. Then the plasma potential V_{pdc}, measured at the powered electrode, is equal to the dc sheath potential at the grounded electrode. Thus, knowing both J_i and V_{pdc}, the sheath thickness d_g can be calculated [Eq. (20)]. Substituting the experimental data obtained at constant power (500 W), values for d_g in the order of 1.5 mm are found. Only small deviations (± 0.15 mm) from this value are observed as a function of B. It follows that at the grounded electrode the sheath thickness is not related to the axial magnetic field by a relation $Bd =$ constant, as was observed at the powered electrode. However, this may be ascribed to the influence of the cusp field. It generates a magnetic-field strength at the surface of the grounded electrode, which is much larger than the axial field. Therefore, variation of the axial field B may have little influence on the sheath thickness.

As reported above, at the powered electrode a value $d_p = 5$ mm was observed when $B = 0$. Thus $d_g < d_p$. Because in addition $A_g > A_p$, it follows from Eq. (19) that at $B = 0$, C_g is considerably larger than C_p. According to Eq. (18) [which states that $V_{dc} = V_{rf}(C_p - C_g)/(C_p + C_g)$], this in good qualitative agreement with the observation of large negative dc offset voltages V_{dc}, which are of the same order of magnitude as the applied generator voltage V_{rf} (see Fig. 17, and also Fig. 14). Going towards larger B values, C_g remains virtually unchanged, whereas the decrease of d_p with $B(B_d = c)$ results in increasing values for C_p. In Fig. 17, the 500-W data for V_{dc} and V_{rf} (from Fig. 10) are replotted, together with the values for V_{dc} which are calculated by substituting C_p and C_g into Eq. (18). Although V_{rf} increasing above 100 G, the calculated values for V_{dc} show a monotonic decrease with B, finally resulting in sign reversal. Thus it is shown that the observed monotonic decrease of V_{dc}, and also its reversing sign, are a direct consequence of the fact that the relative magnitude of both sheath capacitances is reversed by the magnitude field.

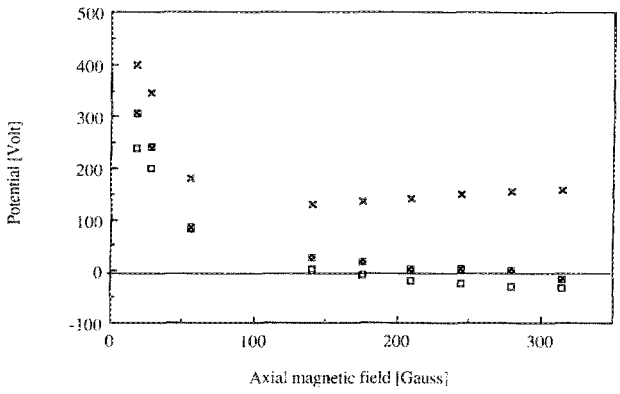

FIG. 17. Measured electrode voltage V_{rf} (crosses) and electrode-offset V_{dc} (open squares), together with calculated values of V_{dc} (filled squares). Calculated data are based on estimated sheath capacitances at the grounded electrode. Measured data taken from Fig. 10.

VIII. CONCLUSIONS

Ion energy distributions have been measured with an electrostatic energy analyzer at the powered electrode of a 13.56-MHz discharge. Plasma confinement by magnetic-cusp fields permits low-pressure discharge operation, resulting in collisionless acceleration of ions in the sheath. Thus, high-resolution energy spectra are obtained. This has been used for an experimental verification of the theory for ion acceleration in rf sheaths, as developed by Vallinga and Meijer. For this purpose, experiments have been performed in absence of an axial magnetic field. Excellent agreement between measured spectra and calculated energy distributions is obtained. From the ion energy distributions, sheath thickness and ion flux towards the wall can be derived. The ion flux, thus calculated, corresponds very well with measured values. In case of high-rf voltages, ion mass resolution is also obtained, resulting from the rf modulation of the sheath potential.

Having established the validity of the model, it has been used to interpret experimental results as a function of axial magnetic-field strength. Application of a variable axial magnetic field results in lower mean ion energies and higher current densities. Both are related to the sheath thickness by the space-charge-limited current equation. The reciprocal sheath thickness behaves linearly with magnetic field, with a slope that is independent of sheath potential and discharge power. This is explained by assuming that the sheath thickness is determined by the Larmor radius of plasma electrons,

and thus only by the electron temperature in the plasma bulk. It implies that rf sheath behavior is principally different from the corresponding dc behavior, which is governed by secondary electrons.

Estimated thickness of the sheath at the grounded electrode lead to the conclusion that the observed sign reversal of the dc offset voltage at the powered electrode is directly related to the relative magnitude of both sheath capacitances. At $B = 0$, the largest sheath capacitance is found at the grounded electrode (which has the largest area). This capacitance changes little upon variation of the axial magnetic field. At sufficiently high magnetic-field strengths (between 200 and 300 G) the capacitance at the powered electrode has increased so much that it exceeds this constant value, resulting in the observed reversal of the offset voltage.

ACKNOWLEDGMENTS

The authors wish to thank P. M. Meijer and W. J. Goedheer (FOM-Institute Rijnhuizen, Nieuwegein) and A. Manenschijn (Delft University of Technology) for stimulating discussions. The work described here was performed as part of the research program of the Stichting voor Fundamenteel Onderzoek der Materie (FOM), with financial support from the Nederlandse Organisatie voor Wetenschappelijk Onderzoek (NWO) and the Dutch Ministry of Economic Affairs within the framework of the IOP-IC program.

[1]S. J. Fonash, Solid State Technol. **28**, 150 (1985).
[2]A. J. van Roosmalen, Vacuum **34**, 429 (1984).
[3]D. L. Flamm and V. M. Donnelly, Plasma Chem. Plasma Proc. **1**, 317 (1981).
[4]G. S. Oehrlein, R. M. Tromp, J. C. Tsang, Y. H. Lee, and E. J. Petrillo, J. Electrochem. Soc. **132**, 1441 (1985).
[5]G. S. Oehrlein, J. Appl. Phys. **59**, 3053 (1986).
[6]J. H. Thomas, J. T. McGinn, and L. H. Hammer, Appl. Phys. Lett. **47**, 746 (1985).
[7]I. Lin, J. Appl. Phys. **58**, 2981 (1985).
[8]S. Bell and T. Bril, Mater. Res. Soc. Symp. Proc. **68**, 53 (1986).
[9]A. D. Kuypers, E. H. A. Granneman, and H. J. Hopman, J. Appl. Phys. **63**, 1899 (1988).
[10]A. D. Kuypers and H. J. Hopman, J. Appl. Phys. **63**, 1894 (1988).
[11]A. D. Kuypers, Ph.D. thesis, University of Utrecht, The Netherlands, 1989.
[12]J. Ero, Nucl. Instrum. **3**, 303 (1958).
[13]C. J. Cook, O. Heinz, D. C. Lorents, and J. R. Peterson, Rev. Sci. Instrum. **33**, 649 (1962).
[14]P. Benoit-Cattin and L. Bernard, J. Appl. Phys. **39**, 5723 (1968).
[15]R. T. C. Tsui, Phys. Rev. **168**, 107 (1968).
[16]Y. Okamoto and H. Tamagawa, J. Phys. Soc. Jpn. **29**, 187 (1970).
[17]J. W. Coburn, Rev. Sci. Instrum. **41**, 1219 (1970).
[18]J. W. Coburn and E. Kay, J. Appl. Phys. **43**, 4965 (1972).
[19]K. Kohler, J. W. Coburn, D. E. Horne, and E. Kay, J. Appl. Phys. **57**, 59 (1985).
[20]F. H. J. Bisschops, Ph.D. thesis, Eindhoven Technical University, The Netherlands, 1987.
[21]P. Briaud, G. Turban, and B. Grolleau, Mater. Res. Soc. Symp. Proc. **68**, 109 (1986).
[22]P. M. Vallinga, P. M. Meijer, H. Deutsch and F. J. de Hoog, in *Proceedings of the XVIII International Conference on Phenomena in Ionized Gases*, edited by W. T. Williams (Hilger, Bristol, United Kingdom, 1987), p. 814.
[23]P. M. Vallinga, thesis, Eindhoven Technical University, The Netherlands, 1988.
[24]J. H. Keller and W. B. Pennebaker, IBM J. Res. Dev. **23**, 3 (1979).
[25]A. Garscadden and K. G. Emeleus, Proc. Phys. Soc. **79**, 535 (1962).
[26]B. Chapman, *Glow Discharge Processes* (Wiley, New York, 1980).
[27]K. Kohler, D. E. Horne, and J. W. Coburn, J. Appl. Phys. **58**, 3350 (1985).
[28]H. R. Koenig and L. I. Maissel, IBM J. Res. Dev. **14**, 276 (1970).
[29]E. H. M. Granneman and M. J. vd Wiel, *Handbook on Synchrotron Radiation*, edited by D. E. Eastman and Y. Farge (North-Holland, Amsterdam, 1983), Vol. 1, Chap. 4.
[30]P. M. Meyer, Internal report VDF/NT 87-04, Eindhoven Technical University, Netherlands, 1987.
[31]A. D. Kuypers and H. J. Hopman, Phys. Lett. A **134**, 480 (1989).
[32]A. Güntherschulze, Z. Phys. **24**, 140 (1924).
[33]J. Willows, Philos. Mag. **6**, 250 (1901).
[34]J. J. Thomson and G. P. Thomson, *Conduction of Electricity Through Gases* (Cambridge University Press, Cambridge, 1933).
[35]A. E. Wendt, M. A. Liebermann, and H. Meuth, J. Vac. Sci. Technol. A **3**, 1827 (1988).
[36]H. Okano, T. Yamazaki, and Horiike, Solid State Technol. **25**, 166 (1982).
[37]H. Kinoshita, T. Ishida, and S. Ohno, J. Appl. Phys. **62**, 4269 (1987).
[38]G. Francis, *Encyclopedia of Physics, Gas Discharges II*, edited by S. Flügge (Springer, Berlin, 1956), Vol. XXII.
[39]S. Maniv, J. Appl. Phys. **63**, 1022 (1988).
[40]M. D. Gill, Vacuum **34**, 357 (1984).
[41]O. A. Popov and V. A. Godyak, J. Appl. Phys. **57**, 53 (1984).
[42]A. D. Richards, B. E. Thompson, and H. H. Sawin, Appl. Phys. Lett. **50**, 492 (1987).
[43]M. J. Kushner, IEEE Trans. Plasma Sci. **PS-14**, 188 (1986).